Classic Force Field for Predicting Surface Tension and Interfacial Properties of Sodium Dodecyl Sulfate

Tao Cheng, Qing Chen, Feng Li, and Huai Sun*

School of Chemistry and Chemical Engineering, Shanghai Jiao Tong University, Shanghai 200240, China

Received: July 27, 2010; Revised Manuscript Received: September 7, 2010

A classical force field capable for accurately predicting surface tensions, surface concentration, and other interfacial properties is reported for sodium dodecyl sulfate (SDS). This force field is proposed by combining parameters from well established force fields for components of the air/SDS/water interface and optimized by adjusting the van der Waals diameter of sulfate oxygen to fit experimental data of surface tension. The force field parameters are transferable; as good agreement with experimental data is achieved from independent calculations on activity derivatives of aqueous solution of sodium methyl sulfate using the Kirkwood−Buff theory. The adjusted parameter effectively modulates the electrostatic interactions of solvated ions in solutions. This modification has a strong impact to surface tension and location and mobility of sodium cations but minimal impact to properties such as density profiles of bulk phase and conformations and orientations of surfactant chain, for which consistent results compared with previous studies are obtained.

1. Introduction

Sodium Dodecyl Sulfate (SDS) is one of the most commonly used anionic surfactant due to its high efficiency in removing oily stains and residues. Apart from its importance in industrial applications, SDS is also of scientific interest as one of the best-studied surfactants. Numerous experimental studies have been reported on thermodynamic and kinetic properties of SDS.[1−7] In parallel, this molecule serves as a popular model for computational studies. Molecular modeling approaches such as molecular dynamics (MD) and Monte Carlo (MC) simulations have been extensively carried out to investigate SDS both in solution and at interfaces.[8−10] Various self-assembly structures depending on the architectures of amphiphiles, temperatures, and presence of other solution components such as dissolved salts were observed in computer simulations.[11,12]

A better understanding of the function and behavior of surfactant requires knowledge of the thermodynamics of amphiphiles.[13] Surface tension is one of the most fundamental thermodynamic properties that characterize the hydrophilic and hydrophobic nature of the surfactant. Prediction of surface tension would be of great interest in surfactant research. However, it is one of the most challenging tasks in molecular simulations.[14] Several calculation methods for predicting surface tension have been developed.[15−17] Biscay et al.[18] had conducted a comparative study of different methods. These authors found that within statistical uncertainties consistent results could be obtained among different calculation methods with appropriate consideration of long-range corrections. One of the most popularly used methods is based on the Kirkwood−Buff formula.[19] Excellent results have been obtained for pure component systems, such as liquid alkane[20] and water.[21] For surfactant air/liquid interface, early attempt for calculating surface tension was reported by Dominguez et al.[22] Successful predictions on interfacial tensions of several popular surfactant solutions were reported by Jang et al.[23,24]

Surface tension is highly sensitive to the force field parameters used in the simulation, which makes it as one of the most critical criterions to evaluate quality of a force field. Models involving ions are difficult to describe using classical force fields in which the point charge model is known to be too crude to represent interactions between ions and molecules.[25,26] Nevertheless, some evidence support the rationality of using nonpolarizable classical models in classical atomistic simulations.[27] Considering the efficiency of simulation, classical force fields with empirically adjusted parameters that effectively represent the complicated interactions are valuable. One of the mostly used nonpolarizable force field for SDS was proposed by Schweighofer et al.[28] In this model, united atoms are used for the hydrocarbon chain, whereas the headgroup (SO_4^-) is described by explicit atoms. Later, Dominguez and Berkowitz[22] added parameters for torsion terms for simulation of SDS in water/oil interfaces. We refer this force field as DB model is this article. The DB model has been widely used by many research groups to study interfacial phenomena and micelles in solutions.[29−38]

However, applying the DB model to calculate surface tensions, we found the surface tensions of air/SDS/water were significantly overestimated. Analysis of the calculated data indicated that the overestimates were mainly due to incorrect descriptions of the ion−ion and ion−water interactions in the complex mixtures. A series of studies showed that properties of aqueous solution were very sensitive to the force field parameters of the monovalence ion.[39−41] Small inaccuracy in the force field parameters would lead to serious errors.[42] The van der Waals (VDW) parameters of ions in the DB model were transferred from the OPLS force field. Its accuracy in representing ions in electrolyte solutions has not been validated.

In this work, we built up a force field by combining parameters from several sources in the literature. We examined how the ionic parameters affect the calculated surface structures and surface tensions by optimizing the most sensitive nonbond parameters using surface tension data as guidance. In addition, activity derivatives of ion solution were employed to validate the transferability of adjusted force field parameters. Using the newly derived parameters, consistent results in both surface

* To whom correspondence should be addressed. Tel.: +86-21-5474-8987-601, Fax: +86-21-5474-1297, E-mail: huaisun@sjtu.edu.cn.

10.1021/jp107002x
Published on Web 10/12/2010

TABLE 1: Nonbond (VDW and Charge) Parameters for SDS

site	ϵ (kJ/mol)	σ (nm)	q ($|e|$)
CH_3[a]	0.8146	0.3750	0.000
CH_2(internal)[a]	0.3824	0.3950	0.000
CH_2(attached to O)[a]	0.3824	0.3950	0.137
$O(SO_3)$[b]	0.8368	0.3150	−0.654
O(COS)[b]	0.7113	0.3000	−0.459
S[b]	1.0460	0.3550	1.284
Na[c]	1.4644	0.2160	1.000

[a] Ref 43. [b] Refs 22 and 28. [c] Ref 45.

tensions and activity derivatives were obtained. We also investigated surface structures and thermodynamics properties and compared the calculated results with previous simulation work and experimental data.

2. Models and Methods

The initial force field parameters were taken from different sources that best describe different fragments of the molecular models. The carbon chain was described by TraPPE united atom force field which has been extensively validated using vapor−liquid equilibrium data of alkanes.[43] Water was described by well-known SPC/E water model.[44] The sodium cation (Na^+) was represented by a set of parameter that specially designed for SPC/E water model.[45] The SO_4^- force field parameters were taken from the DB model. The combined force field parameters were listed in Table 1.

The potential energy function is in AMBER form:

$$E = \sum_{\text{bonds}} K_r(r - r_0)^2 + \sum_{\text{angles}} K_\theta(\theta - \theta_0)^2 + \sum_{\text{torsions}} \frac{V_n}{2}[1 + \cos(n\phi - \gamma)] + \sum_{i<j}^{\text{atoms}} 4\varepsilon_{ij}\left[\left(\frac{\sigma_{ij}}{r_{ij}}\right)^{12} - \left(\frac{\sigma_{ij}}{r_{ij}}\right)^{6}\right] + \sum_{i<j}^{\text{atoms}} \frac{q_i q_j e^2}{r_{ij}} \quad (1)$$

The five terms in the above equation compute the energies of bond stretching, angle bending, torsion angles, and nonbonded van der Waals and electrostatic interactions, respectively. Detailed explanations on the parameters in the above equation can be found elsewhere.[46]

Unlike-atom interactions are computed using standard Lorentz−Berthelot combination rules

$$\sigma_{ij} = (\sigma_{ii} + \sigma_{jj})/2 \quad (2)$$

$$\varepsilon_{ij} = \sqrt{\varepsilon_{ii}\varepsilon_{jj}} \quad (3)$$

Scaling factors of 1/1.20 is used for the 1−4 intramolecular electrostatic interaction and 1/2.0 is used for the 1−4 van der Waals interaction.

A double-monolayer model with SDS surfactants adsorbed at the air/water interfaces was built as the basic simulation model in this work. The initial configuration of this model was set up by arranging surfactants on each monolayer with sulfate (SO_4^-) group placed toward the water phase, and the hydrocarbon chains were in fully extended conformation perpendicular to this surface plane. Normally, the surface area was fixed at 3.1 × 3.1 nm^2. With 23 surfactants, this setting yields 0.42 nm^2 surface area per molecule, corresponding to experimentally observed value of interface adsorption at CMC.[24] The z direction of the simulation box was kept at 20 nm. The simulation box contained 46 surfactants and 1706 water molecules, which correspond to a thickness of 8 nm for the double-faced liquid phase. To simulate the surface tension isotherms, the z dimension of simulation box was reduced to 14 nm for efficiency. A larger simulation box, 4.1 nm × 4.1 nm × 16.0 nm with 4000 water, 80 surfactants, and 80 Na^+, was used to investigate the cutoff effect. The initial configurations were equilibrated at constant volume and at 298 K for 2 ns, followed by production run of 2 ns duration. All simulations of interfaces were performed in the canonical (NVT) ensemble at 298 K.

Surface tension was calculated by applying Kirkwood−Buff formula, a general method for computing surface tensions using molecular simulations originally developed by Tolman[47] and refined by Kirkwood and Buff.[19] The surface tension is calculated as an integral of the difference between the normal and tangential pressure P_N and P_T:[20]

$$\gamma_P = \frac{1}{2}\int_{-\infty}^{\infty}(P_N(z) - P_T(z))\mathrm{d}z \quad (4)$$

where z is along the direction normal to the interface, $P_N(z) = P_z(z)$ and $P_T(z) = (P_x(z) + P_y(z))/2$. In bulk liquid, $P_N = P_T$ and the integrand vanishes; therefore, the nonzero contributions to the integral come from the interfacial region only. For an interface between two fluid phases, the integral in equation can be replaced with an ensemble average of the difference between the normal and tangential pressures:

$$\gamma_P = \frac{L_z}{2}\langle P_N - P_T\rangle = \frac{L_z}{2}\left[\langle P_z\rangle - \frac{\langle P_x\rangle + \langle P_y\rangle}{2}\right] \quad (5)$$

The outer factor of $^1/_2$ in eq 5 accounts for the presence of two liquid−vapor interfaces, which is used in modeling the liquid−vapor interface with the periodic boundary conditions.

To validate force field parameters, aqueous solutions of CH_3SO_4Na (sodium methyl sulfates) were prepared and activity derivatives were calculated. Two concentrations of the solute, 1.2 and 3.1 M, were taken into consideration. This was achieved by placing 46 and 139 CH_3SO_4Na in 2000 water molecules. Initial configurations of different solutions were generated by randomly inserting waters, $CH_3SO_4^-$ and Na^+ into a cubic box with side length of 5 nm, using *PACKMOL*.[48] The steepest descent method was then used to perform 1000 steps of minimization. This was followed by extensive equilibration with time of typically 4 ns, and data collection of more than 1 ns. Averages of properties and standard deviations were calculated from three (3) independent simulations. Simulations of the aqueous solutions were performed in the isothermal isobaric (NpT) ensemble at 298 K and 1 atm.

The Kirkwood−Buff theory was used to calculate activity depravities. The details of this theory can be found in the literature.[49] Here, we give a short description based on Weerasinghe's work[50] for complete information. The thermodynamic properties of a mixture solution can be expressed in terms of the *KB* integrals (G_{ij}) between different components i and j

$$G_{ij} = 4\pi\int_0^{\infty}[g_{ij}^{\mu PT}(r) - 1]r^2\mathrm{d}r \quad (6)$$

Here, $g_{ij}^{\mu vt}(r)$ is radial distribution function (RDF) in the μVT ensemble, and r is the corresponding center-of-mass to center-of-mass distance between components i and j. *KB* integrals can be evaluated from the simulation data (*NPT* ensemble) by assuming that,

$$G_{ij} = 4\pi \int_0^{\infty} [g_{ji}^{\mu PT}(r) - 1] r^2 \mathrm{d}r \qquad (7)$$

where R represents a correlation region beyond which the RDF converged to unity.

For a binary solution consisting of water (w) and a cosolvent (c), a variety of thermodynamic quantities can be defined in terms of the KB integrals G_{ww}, G_{cc}, and $G_{cw} = G_{wc}$, and the molar concentrations ρ_w and ρ_c. The derivative of the cosolvent activity α_{cc} is given by:

$$\alpha_{cc} = \frac{1}{1 + \rho_c(G_{cc} - G_{cw})} \qquad (8)$$

For computation of activity derivatives, we followed the literature[50] by treating the ternary salt solution as a binary system of indistinguishable ions and water. Consequently, for a 1:1 salt one has the molar concentrations of cosolvant as $\rho_c = 2C_s$ (C_s is the mole concentration of salt concentration). The experimental activity coefficients for sodium methyl sulfates solutions were taken from the data measured by Gampe et al.[51] In their work, the activity coefficients for these solutions were determined at 298 K by the isopiestic method. From the activity coefficients data, the activity coefficient derivatives were obtained analytically.

All simulations were carried out using *Gromacs 3.3.3*.[52] Berendsen[53] weak coupling technique was used to modulate the temperature and pressure with relaxation times of 0.1 and 0.5 ps, respectively. A 1 fs time step for integration of the equations of motion was chosen. The particle mesh Ewald[54] technique was used to evaluate electrostatic interactions. A real space convergence parameter of 3.5 nm was used in combination with a cutoff of 1.0 nm of VDW interactions for solution simulations and 1.5 to 2.0 nm for interface simulations. The nonbond list was updated every 5 steps. The reciprocal space sum was evaluated with 0.12 nm resolution.

3. Results and Discussions

3.1. Surface Tensions. Calculation of surface tension requires consideration of a number of simulation conditions, such as size effect,[17,55] the periodic conditions,[17,56] the range of interactions,[57−60] and the truncation effect involved in the calculation of potential energy and force.[57,61,62] Biscay et al[63] published a good review on these issues. Among these factors, the simulation size and the range of interactions are the most critical for calculating surface tensions.

For simulation size, it was demonstrated by different authors[55,63] that the surface tension is subjected to oscillations with respect to the interfacial area and the length of the dimension perpendicular to the surface. It is established that in order to avoid finite-size effects, the surface area should be greater than $9 \times 9\ \sigma^2$ (where σ is the dimension of molecule).[63] For the perpendicular dimension, the liquid layer must be thick enough to avoid a significant dependence of surface tension with the simulation dimension. Biscay et al[63] recommended a value of 50 σ for the length (L_z) on the perpendicular dimension and 13 σ for the thickness of the liquid layer. In this work, the area of interface was 3.1 × 3.1 nm^2, L_z was between 14 to 20 nm, and the liquid phase thickness was 8 to 10 nm. Using water dimension, these numbers correspond to $10 \times 10\ \sigma^2$ in $X-Y$ direction, 44σ to 63 σ in L_z, and 25σ to 32σ in liquid phase.

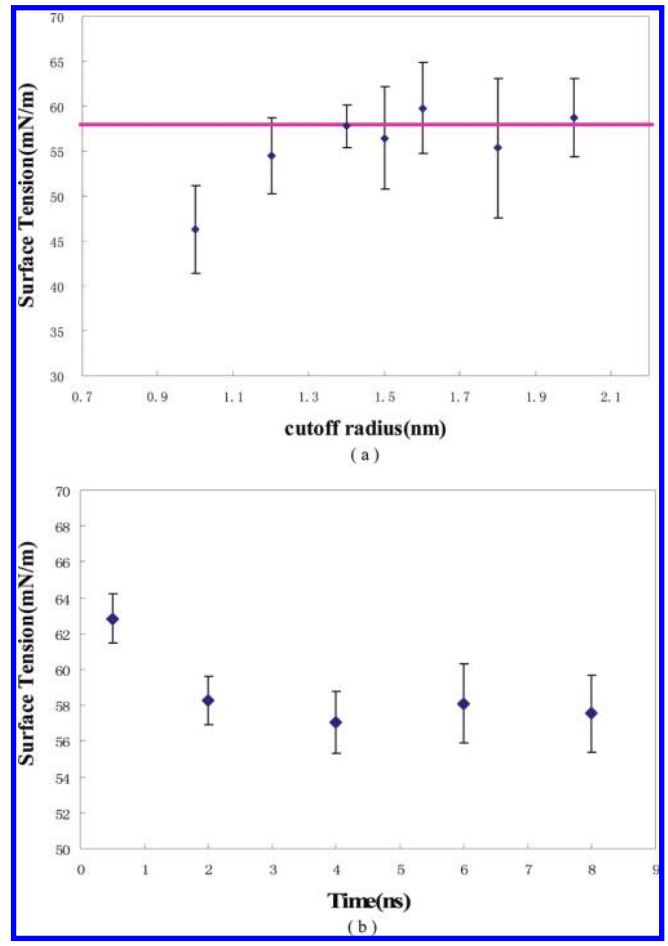

Figure 1. (a) Surface tensions calculated for air/SDS/water monolayer with different cutoff radius. The horizontal line stands for the average value using data after 1.4 nm. (b) Surface tensions results as a function of simulation time with a 1.5 nm cutoff.

To consider the factor of long-range nonbond interaction, we carried out a series of simulations on the air/SDS/water interfaces and calculated surface tensions with different cutoff radius with DB force field. Part a of Figure 1 shows the simulated surface tensions as functions of the cutoff radius ranging from 1 to 2 nm using the composed initial force field. For each point, the calculated uncertainty is indicated by the error bar. There is a substantial increase from 1.0 to 1.4 nm, followed by stabilized data around an average value indicated by a horizontal line. This indicates that for this system a minimum cutoff of 1.4 nm is required. Considering parameter change may have an impact to the required cutoff value, we chose a cutoff value of 1.5 nm, which is larger than the minimum requirement in the rest of this work. The long-range correction (LRC) contribution has been discussed in literature.[59,61,62,64] However, evidence shows that for high polar system, such as water, the LRC was negligible comparing with fluctuation.[65] As shown by our results, the variation of the calculated data after 1.4 nm cutoff is smaller than the error bars, which measure the computational fluctuations.

The production time for obtaining converged surface tension was investigated. Part b of Figure 1 shows the calculated surface tensions as a function of the production time. For a well-

TABLE 2: Comparison of Surface Tensions Calculated Using Different $\sigma_{O(SO3)}$

	Surface Tension (mN/m)			
delta (nm)	valence	vdW	electrostatic	Total
0.315	170	−265	154	59(3)
0.325	148	−227	129	51(4)
0.340	140	−183	83	40(3)
0.350	111	−138	60	33(2)
Exp.				38.4

equilibrated simulation, 2 ns production time is required to obtain consistent surface tensions with 1.5 nm cutoff.

Using the protocol discussed above, the surface tension of air/SDS/water interface is calculated with DB force field. Because the original article did not clarify how to combine the interaction between different types of molecules, two commonly used combination rules are investigated here. One is Lorentz−Berthelot (LB) combining rule which uses arithmetic average for the vdW radius and geometric average for the well depth, and the other is geometric mean combining rule, which uses geometric average for both the vdW radius and the well depth. Using the geometric mean combining rules, the calculation result was 60 (1) mN/m and using LB combining rules the calculation result was a little larger, 63(2) mN/m. Both of these data are much greater than the experimental data of 38.4 mN/m, measured at the same surface concentration.[24] Recent researches revealed that LB combining rules, which can properly account for the excluded volumes of ions, are better for reproducing the experimental trend.[66,67] We used LB combining rules in this work.

Using the composed initial force field, the calculated surface tension is 59(3) mN/m (as shown Table 2), slightly lower than that calculated by the DB model, but still too high to compare with the experimental data.

3.2. Force Field Parameters. At the air/SDS/water interfaces, the surfactants are self-assembled to form monolayer with tails in contact with air (vacuum in this work). There are three domains of concentration in the system: the surfactant tails, surfactant heads which interact with water, and water bulk. The interactions among hydrocarbon chains in the surfactant tail region and water−water interactions in bulk liquid are well described by the corresponding force fields (TraPPE and SPC/E respectively). The parameters for hydrophilic group (SO_4^-) and countercation (Na^+) are central to describing the interface. Among numerous Na^+ force field parameters reported, the parameters reported by Suk Joung et al.[45] were specially designed for SPC/E model, which could well produce the hydration free energy. Therefore, only parameters for the SO_4^- group have not been rigorously tested.

The initial VDW and charge parameters were taken from the DB model. As the headgroup is highly charged (−0.654e on each oxygen), the electrostatic interactions dominate the interactions. The strength of these interactions strongly depends on atom−atom distance. A simply sensitivity analysis shows that the predicted interaction energy would be very sensitive to the VDW diameter parameters of the outside oxygen atoms as they are directly correlated to the atom−atom distances. Consequently, we focused on the VDW diameter of sulfate oxygen $\sigma_{O(SO3)}$ to optimize the force field.

Surface tensions calculated for the water/SDS/air interface using different values of $\sigma_{O(SO3)}$ ranging from 0.315 to 0.350 nm are listed in Table 2. As expected, the calculated surface tension is very sensitive to the $\sigma_{O(SO3)}$ parameter. As the $\sigma_{O(SO3)}$ increases from 0.315 to 0.350 nm, the calculated surface tensions change from 59 to 33 mN/m. At $\sigma_{O(SO3)} = 0.340$ nm, the result of 40(3) mN/m is in close agreement with the experimental data of 38.4 mN/m.

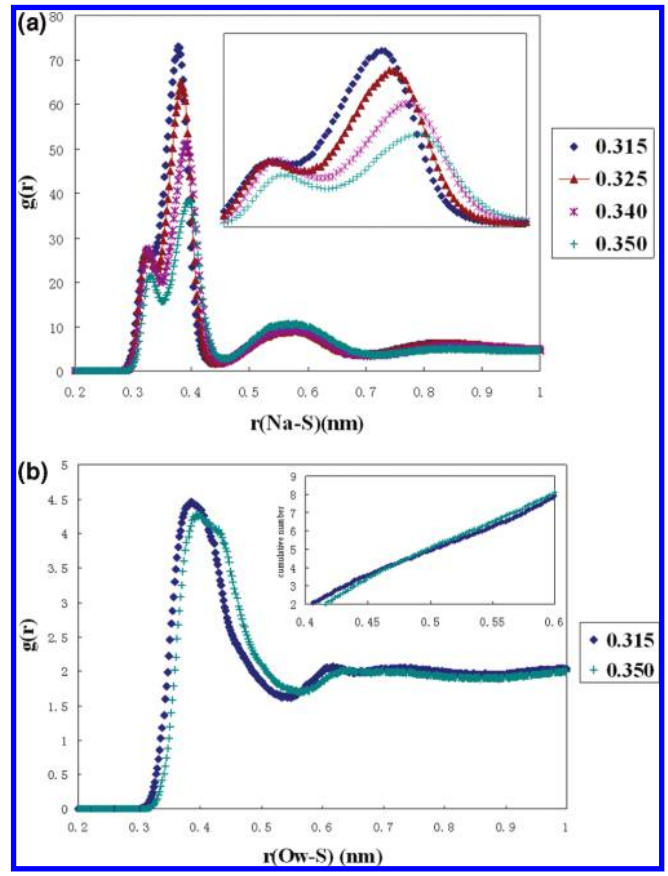

Figure 2. Pair radial distribution functions of (a) Na−S(SO_4) and (b) O(water)−S(SO_4) in the air/SDS/water interface with different parameters of $\sigma_{O(SO3)}$. Insert of (a) is the enlargement between 0.3 nm to 0.45 nm. Insert of (b) is the cumulative number of water molecules between 0.4 to 0.6 nm.

The calculated surface tensions are strongly correlated with the liquid structures at the interface, especially the distribution of sodium cations. Part a of Figure 2 shows RDFs of Na−S(SO_4^-) calculated with different $\sigma_{O(SO3)}$ values. The RDFs show three peaks, two peaks are at the short range, locating at 0.34 nm and 0.40 nm respectively, and one broad peak locates from 0.50 nm to 0.65 nm. The insert figure is the enlargement of the first and second peaks. The first peak is consistent with that observed at SDS crystal,[68] which reflects a salt bridging structure. Comparing with the salt bridging peak, the second peak, which corresponds to the first layer of absorbed Na^+ is more important. As the value of $\sigma_{O(SO3)}$ increases, the heights of the second peaks decrease monotonically, indicating that the short-range structures become less ordered as $\sigma_{O(SO3)}$ increases. For the third peak, as the $\sigma_{O(SO3)}$ radius increases, its height increases a little. Meanwhile, as $\sigma_{O(SO3)}$ increases, an obvious tendency is that the positions of three peaks shift to longer distance.

The shift to longer distance of the Na−S(SO_4^-) peaks is significant. As $\sigma_{O(SO3)}$ increases from 0.315 to 0.350 nm, Na−S(SO_4) distances move 0.021 nm further (from 0.377 to 0.398 nm). But the effect to interaction energy is nontrivial. Simple energy analysis shows that this 0.021 nm shift would reduce electrostatic interaction of two opposite charged particles as much as 20 kJ/mol. This reduction of electrostatic interaction energy has an important impact to the structure at interface.

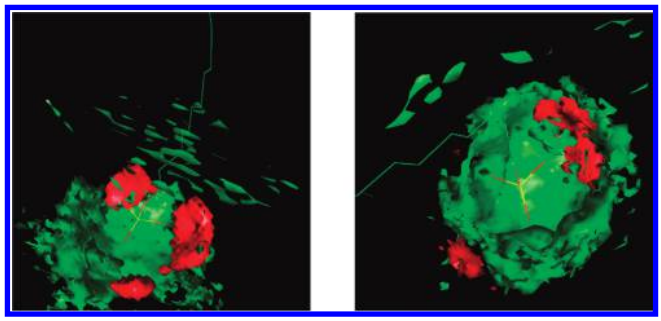

Figure 3. 3D spatial distribution functions of sodium (in red) and water (in green) for SDS. (left) sodium−sulfate interaction dominates ($\sigma_{O(SO3)}$ 0.315 nm); (right) water−sulfate interaction dominates ($\sigma_{O(SO3)}$ 0.350 nm).

More Na^+ would diffuse to bulk phase, which can be directly seen from the weakening of peak heights for the first and second peak and enhancement of the peak height of the third peak. In the same time, more water would be absorbed around SO_4^- anions to replace the Na^+ cations.

The increased population of water molecules near the anionic heads can be verified by structural analysis. The RDFs of O_w(water)−S(SO_4^-) given in part b of Figure 2 shows mild changes as the parameter $\sigma_{O(SO3)}$ changes from 0.315 to 0.350 nm. The first peak is slightly shifted to a longer distance as $\sigma_{O(SO3)}$ increases. However, the height of the peak is almost unchanged and the peak is slightly wider, implying that the water molecules are not repelled away from the head groups as the parameter $\sigma_{O(SO3)}$ increases. The calculated cumulative number of water molecules between 0.4 to 0.6 nm (insert of part b of Figure 2) confirms this argument. As more sodium cations are driven away from the head groups, relatively more water molecules are populated in the first shell of the surfactant headgroup. This can be clearly seen from the spatial radical functions of surfactant hydrophilic group, as given in Figure 3. The green and red colors indicate probabilities of finding water and Na^+ respectively, and the surfactant molecule is displayed as colored lines (green, carbon; yellow, sulfur; and red, oxygen). Two figures calculated with $\sigma_{O(SO3)}$ = 0.315 and 0.315 nm respectively are displayed for comparison. At $\sigma_{O(SO3)}$= 0.315 nm, the interactions among ions are strong, and each surfactant hydrophilic group is in close contact with Na^+. As $\sigma_{O(SO3)}$ is increased to 0.350 nm, the interaction between the ions are weakened. More water and less Na^+ are found near the surfactant headgroup. The Na^+ cations and SO_4^- anions are separated by water molecules; hence, increase $\sigma_{O(SO3)}$ parameter effectively represents the water shielding of the point charges.

Because a change of parameter led to change of liquid structure, there is no simple relationship between the changed parameter and energy components in calculated surface tensions. We calculated the contributions to surface tensions in terms of valence, vdW and electrostatic interactions, and the results are tabulated in Table 2. Both the valence and the electrostatic interactions have a net positive contribution but vdW results in a negative contribution. As $\sigma_{O(SO3)}$ increases from 0.315 to 0.350 nm, the components of valence and electrostatic terms decrease steadily. In the same time, the component of vdW terms increases, which offsets the decreases attributed to the valence and electrostatic terms. As a result, the total surface tension decreases in a mild way.

3.3. Activity Derivatives. To validate the proposed modification of parameters, we extended simulations to aqueous CH_3SO_4Na solutions, in which the $CH_3SO_4^-$ group represents the most important part of SDS surfactant. The force field

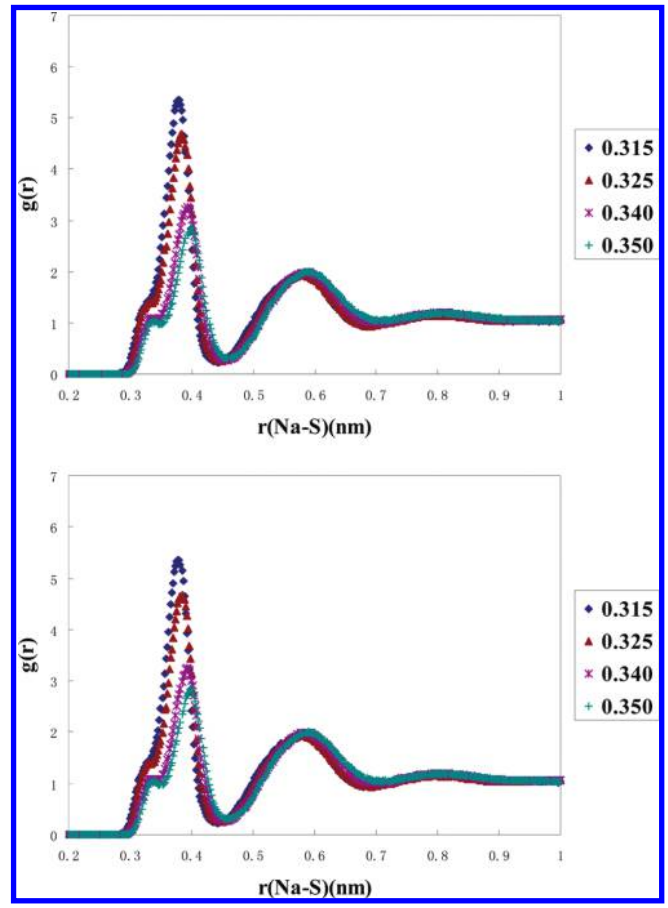

Figure 4. Pair radial distribution functions of Na−S(SO_4) in 1.2 M (top) and 3.1 M (bottom) $CH_3(SO_4)Na$ solution, using models with different $\sigma_{O(SO3)}$, 0.315 nm, 0.325 nm, 0.34 nm, and 0.35 nm.

parameters were transferred from SDS. The only modification is CH_3 group has 0.137 positive charges to keep the neutrality. We carried out simulations at two concentrations of CH_3SO_4Na, 1.2 and 3.1 M.

Figure 4 shows RDFs of Na−S(SO_4) calculated using different $\sigma_{O(SO3)}$ values and on different concentrations. The shapes of the RDFs are similar to that obtained for the interface monolayer. As the $\sigma_{O(SO3)}$ value increases, the heights of first and second peaks decreases, and the positions of these peaks shift to right. The positions of peaks are nearly the same for two salt concentrations. The only difference is the amplitude of changes. For the case of high concentration, its RDFs show more structured features and the RDFs are more sensitive to the parameter changes.

The KB integrals were calculated from the RDFs. A well-known problem for computing the KB integral is about poor convergence. Figure 5 shows the calculated KB integral values for the 3.1 M solution as a function of integral distance. The KB integral fluctuates dramatically as the integral range increases, showing signs of convergence when the integral distance reaches 0.8 nm. However, the convergence is more evident for G_{cw} than that for G_{cc}. The latter suffered from lower samplings as the number of cosolvent ($CH_3SO_4^-$) molecules is far less than the number of water molecules. Following previous work of Weerasinghe,[50] the average value calculated between 0.85 and 1.20 nm was used as the integral value.

The activity derivatives (a_{cc}) calculated using different $\sigma_{O(SO3)}$ values for CH_3SO_4Na electrolyte solutions at two concentrations are summarized in Tables 3 and 4. Properties listed are density, mole concentration, G_{cc}, and G_{cw}. To compare with the

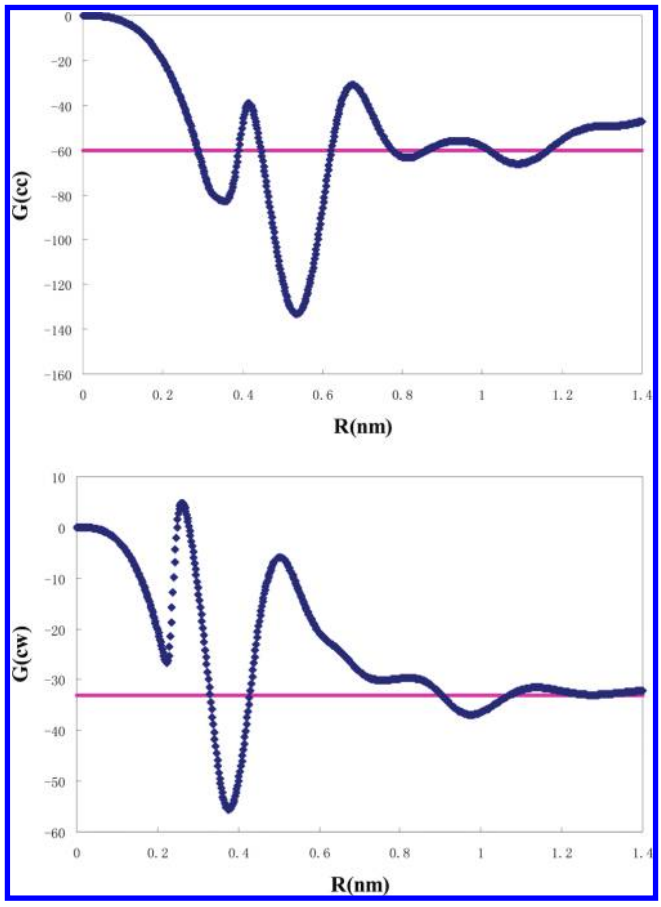

Figure 5. Kirkwood−Buff integrals (cm^3/mol) as a function of integration distance R obtained from the 3.03 M simulation with $\sigma_{O(SO3)}$ 0.340 nm. The thin horizontal lines correspond to the values obtained after averaging $G_{ij}(R)$ between 0.85 and 1.2 nm.

TABLE 3: Comparison of Properties of 1.2M CH_3SO_4Na Aqueous Solution Obtained with Different $\sigma_{O(SO3)}$

property	0.315	0.325	0.340	0.350	Exp.
density (g/cm^3)	1.08	1.08	1.07	1.07	
C_s (M)	1.18	1.18	1.17	1.17	
m (mol/kg)	1.10	1.09	1.10	1.09	
G_{cc} (cm^3/mol)	−4	−77	−49	−75	
G_{cw} (cm^3/mol)	−33	−30	−35	−32	
α_{cc}	0.9(1)	1.1(1)	1.0(1)	1.1(2)	0.99

TABLE 4: Comparison of Properties of 3.1 M CH_3SO_4Na Aqueous Solution Obtained with Different $\sigma_{O(SO3)}$

property	0.315	0.325	0.340	0.350	Exp
density (g/cm^3)	1.21	1.20	1.18	1.17	
C_s (M)	3.11	3.08	3.03	3.00	
m (mol/kg)	2.57	2.57	2.57	2.56	
G_{cc} (cm^3/mol)	76	−12	−60	−92	
G_{cw} (cm^3/mol)	−61	−42	−33	−25	
α_{cc}	0.54(4)	0.8(2)	1.1(2)	1.7(1)	1.11

experimental data, weight concentrations are also listed. Table 3 shows the properties at 1.2 M. The density of the solution is 1.08 g/cm^3, a little higher than that of water. All of the four sets of calculations show similar result of G_{cw} around −33, and various G_{cc} obtained from −4 to −77. The force field parameter does not show obvious tendency in calculating activity derivatives. All of the calculated a_{cc} are around 1.0, which is in good agreement with the experimental data of 0.99.[51] The $\sigma_{O(SO3)}$ value has little effect in calculating activity derivatives at low concentration.

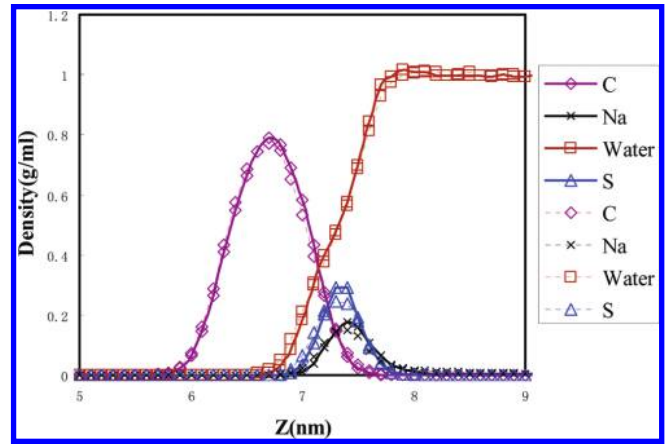

Figure 6. Atomic density profiles for the alkyl chain (C), Na^+, water, and S. The symbols are listed in the figure. Solid line refers to $\sigma_{O(SO3)}$ 0.315 nm and slash line refers to $\sigma_{O(SO3)}$ 0.340 nm.

At higher concentration, the activity derivatives are more sensitive to the force field parameter. As the $\sigma_{O(SO3)}$ increases, the density of solution decreases from 1.21 g/cm^3 to 1.17 g/cm^3, the mol concentration is decreased from 3.11 to 3.00 M, correspondingly. Significant changes are observed for G_{cc} and G_{cw}. As the $\sigma_{O(SO3)}$ value increases, G_{cc} decreases from 76 to −92. At $\sigma_{O(SO3)}$ = 0.315 nm, a positive G_{cc} is obtained, indicating a preference of strong association among ions. As the $\sigma_{O(SO3)}$ parameter increases, the tendency of dissociation of ions is reflected by negative values in G_{cc}, which naturally attributes to weakening of ion interactions. G_{cw} shows a steady increase along with the increment of $\sigma_{O(SO3)}$, ranging from −61 to −25, indicating gradually increased association of water with ions. Both the decrease of G_{cc} and increase of G_{cw} led to significantly increased values of the calculated activity derivatives from 0.54 to 1.7. At $\sigma_{O(SO3)}$ =0.340 nm, a_{cc} at both 1.2 and 3.1 M agree well with the experimental data, consistent with the surface tension results.

3.4. Additional Properties. Figure 6 shows the Z-dependent atom-density distributions $\rho(Z)$ of united atom carbons, Na^+, water and S at $\sigma_{O(SO3)}$ = 0.315 nm and $\sigma_{O(SO3)}$ = 0.340 nm. The primary features of the density profiles are similar to previous simulations of the surfactant monolayer at interface.[28] The head groups are dissolved in the water, whereas the alkyl chains are excluded from the interface and little water penetrate into the alkane chain. Comparison of the curves obtained using two sets of parameters shows that the profiles of water and alkyl chains are nearly the same, indicating that the bulk phase and thickness of the interface are not strongly influenced by the changes of ions parameter. Significant differences can be observed for Na^+ and S distributions. With positions of the peaks nearly the same, the distribution is narrower with $\sigma_{O(SO3)}$ = 0.315 nm, indicating the mobility of ions are more restricted.

The ordering of the tails in surfactant membranes is characterized by the order parameter S,[69] which shows the average inclination of the tail orientation with respect to the surface normal. The S order parameter for the ith atom is calculated using the following formula:

$$S = (1/2)\langle 3(\cos\theta_i)^2 - 1\rangle \quad (9)$$

Where θ_i is the angle between the ith molecular axis and the normal to the interface. Order parameters varies between 1 (full order along the interface normal) and $-1/2$ (full order perpen-

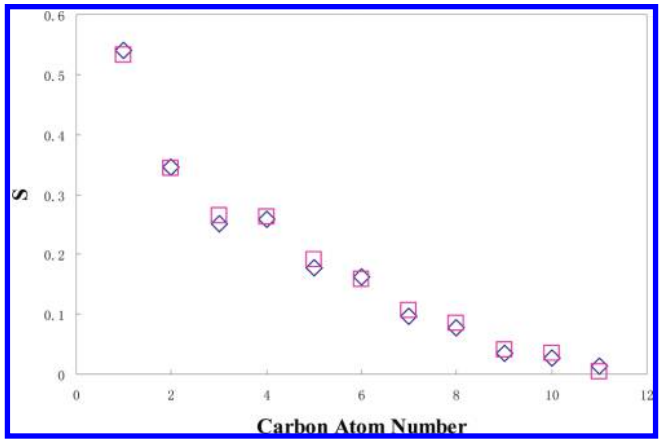

Figure 7. *S* order parameter as a function of the carbon position. The blue diamonds refer to $\sigma_{O(SO3)}$ 0.315 nm; the pink squares refer to $\sigma_{O(SO3)}$ 0.340 nm.

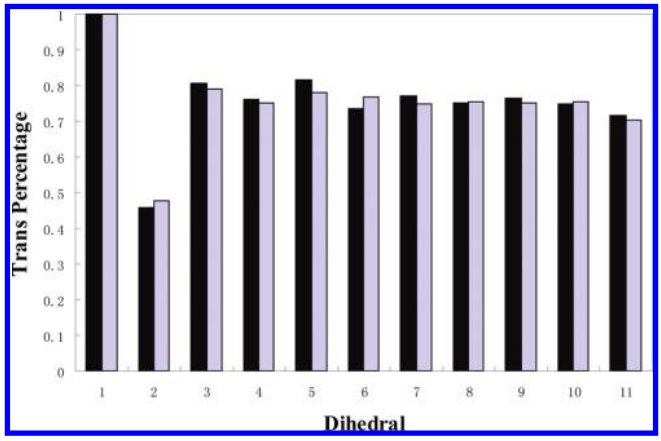

Figure 8. Trans statistics for the eleven (11) dihedral angles in the backbone of the sodium dodecyl sulfate. Dihedral no. 1 involves the sulfur atom and the three atomic sites behind it. Dihedral no. 11 refers to the endmost dihedral angle in which the terminal methyl group is a member. The black bars refer to $\sigma_{O(SO3)}$ 0.315 nm; the gray bars refer to $\sigma_{O(SO3)}$ 0.340 nm.

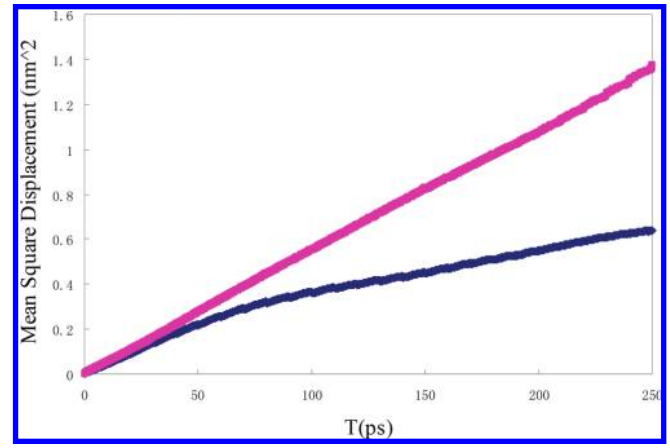

Figure 9. Mean square displacement of Na^+ as a function of time. The blue points refer to $\sigma_{O(SO3)}$ 0.315 nm; the pink points refer to $\sigma_{O(SO3)}$ 0.340 nm.

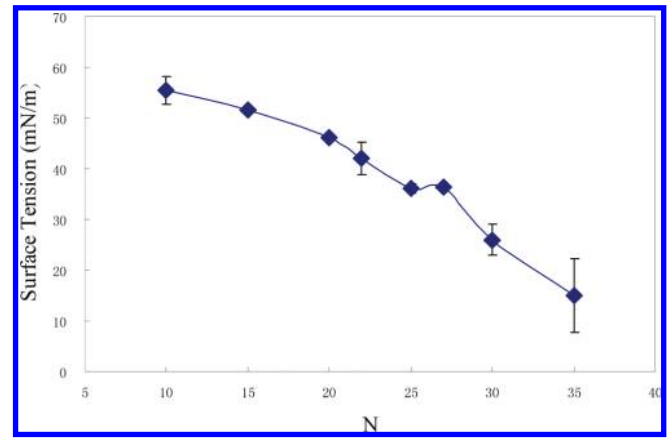

Figure 10. Surface tension isotherms for SDS.

dicular to the normal), with a value of zero in the case of isotropic orientation.

Figure 7 show the *S* order parameters of SDS carbon chain calculated for systems with $\sigma_{O(SO3)}$ 0.315 nm and $\sigma_{O(SO3)}$ 0.340 nm, respectively. The carbon atoms are numbered starting from the headgroup. The *S* order parameters decrease rapidly for the first two carbon atoms, followed by a plateau extending through carbon atoms 3, 4. From carbon 5, the *S* parameter decrease continually. The *S* order parameter is nearly zero at the end. The large *S* parameter of the first two carbon atoms attribute to the steady orientation caused by group interactions of the head groups with solvent. The alkyl chains are rather flexible and nearly orient randomly. The two curves are nearly identical, which indicates that the modified force field parameter have little impact to the chain orientations. This is consistent with above discussions.

The bar graph in Figure 8 shows the percentage of trans configurations for each dihedral angles on the alkyl chain of SDS. The black bars denote $\sigma_{O(SO3)} = 0.315$ nm and gray bars represent $\sigma_{O(SO3)} = 0.340$ nm, respectively. The dihedral angles are numbered from the head. There are eleven (11) dihedral angles, and the first dihedral angle consists of atoms $S-O-C(H_2)-C(H_2)$. Most of these dihedrals are in trans, only about 25% in gauche, which suggests that the carbon chains are rather extended. The first dihedral is completely in trans, consistent with previous study,[28] which have been explained as the steric inhibition and preference to form hydrogen bonds for the head groups. The second dihedral angle shows unusually large portion in gauche. This defect causes the alkyl chains turn to vertical orientation of the interface, which has been validated by experimental observation.[70] Despite trivial differences, the dihedral distributions obtained by two set of parameters $\sigma_{O(SO3)}$ are nearly the same, which indicates that the change of the parameter has little effect on the configurations of alkyl chain.

Figure 9 showed the mean square displacement of Na^+ as a function of time for $\sigma_{O(SO3)} = 0.315$ nm (blue) and $\sigma_{O(SO3)} = 0.340$ nm (pink). The self-diffusion coefficients of Na^+ at room temperature are 0.3(2) and 0.8(3) $10^{-5}cm^{2s-1}$, respectively. Both are lower than that of Na^+ in bulk water ($1.24 \times 10^{-5}cm^2s^{-1}$),[71] reflecting that the mobility of Na^+ is generally restricted at interfaces due to the formation of electric double layers[13] of SO_4^- and Na^+, respectively. Comparison of the results obtained using two sets of parameters indicate that the change of force field parameter has a strong impact to the mobility of Na^+, as the self-diffusion coefficient is more than doubled.

Figure 10 shows the calculated surface tensions isotherm as a function of surface concentrations. This plot can be divided into three regions. From $N = 10$ to $N = 25$, surface tension decreased gradually as more surfactant placed at interface. A small plateau is observed between $N = 25$ and $N = 27$. After $N = 27$, the calculated surface tension continue declining rapidly. It is of interest to note that the surface tension of 39(6) mN/m at the plateau is in excellent agreement with the experimental data of 38 mN/m. In addition, the plateau

corresponds to surface concentrations of 35.59−38.44 Å^2, which compare favorably with the experimental result of 33−52 Å^2.

The trend between $N = 5$ and $N = 27$ is in agreement with experimental observation. At low concentration, surfactant molecules are adsorbed at the interface predominately, but the ability of deceasing surface tension is limited due to few number of surfactant molecules. As more surfactants are added, greater interface area is covered and surface tension continue decreasing. When a relatively stable monolayer structures is achieved, small perturbations have little influence on the surface tension. When $N > 27$, the simulation model cannot represent the experimental reality as the double monolayer computational model does not allow formation of micelles, whereas in reality the surfactant molecules enter bulk to form micelles when the surface is saturated. To simulate the equilibrated formation of monolayer and micelles, a much larger length scale and more efficient simulation method, such as a Monte Carlo simulation, would be required.[72]

Conclusions

A new force field is proposed by combining parameters from well established force fields for components of the air/SDS/water interface and optimized using surface tensions as guidance. Although the force field is based on the fixed-charge model, excellent results of surface tension have been obtained. The calculated surface tensions are correlated with the surface concentrations. A plateau on the surface tension isotherm curve is observed where both surface concentration and surface tension agree well with experimental data.

The force field parameters are transferable as demonstrated by independent calculations on activity derivatives of components of aqueous sodium methyl sulfate solutions using the Kirkwood−Buff theory. The results obtained for both concentrations (1.2 and 3.1 M) agree well with experimental data. The high-concentration data show strong dependence to the force field parameter, as association and dissociation behavior of ions are more sensitive to amplitude of their interaction. Also, as concentration increasing, changes of G_{cc} and G_{cw} would lead to more distinctive changes in a_{cc}, which can be seen from eq 8.

The optimization of force field was done by adjusting only one parameter − the VDW diameter of oxygen of the sulfate group ($\sigma_{O(SO3)}$). The reason of adjusting one VDW parameter works is that the parameter effectively modulates electrostatic interactions. The point charge model is inadequate for representing the whole range of ionic interactions in water. The solvated Na^+ interacts with the solvated sulfate anion SO_4^- in a very complex way. Although the point charge model represents middle and long-range electrostatic interaction well, it overestimates the short-range interaction. By increasing the $\sigma_{O(SO3)}$ parameters slightly, the interaction between Na^+ and SO_4^- is damped, and the average distance between sulfate oxygen and Na^+ is increased, which effectively represent the salvation effect on Na^+, resulting excellent agreement of surface tension, further validated by reproducing a_{cc}.

The reduced electrostatic interaction has a strong impact to the location and mobility of sodium cations. More Na^+ cations enter the bulk phase. The self-diffusion coefficient of Na^+ in solution is more than doubled as the parameter has been changed. However, the modification has minimal impact to density profiles of bulk phases, conformations, and orientations of surfactant chain. Therefore, consistent results comparing with precious predictions on the structures of surfactant molecules are obtained.

Acknowledgment. Financial support from the National Science Foundation of China (No. 20473052), NSAF funding (No. 10676021), and National Basic Research Program of China (No. 2003CB615804 and 2007CB209701) is gratefully acknowledged.

References and Notes

(1) Varadaraj, R.; Bock, J.; Valint, P.; Zushma, S.; Thomas, R. *J. Chem. Phys.* **1991**, *95*, 1671.
(2) Wormuth, K. R.; Zushma, S. *Langmuir* **1991**, *7*, 2048.
(3) Conboy, J. C.; Messmer, M. C.; Richmond, G. L. *J. Chem. Phys.* **1996**, *100*, 7617.
(4) Gelbart, W. M.; Ben-Shaul, A. *J. Chem. Phys.* **1996**, *100*, 13169.
(5) Conboy, J. C.; Messmer, M. C.; Richmond, G. L. *J. Chem. Phys. B* **1997**, *101*, 6724.
(6) Widera, B.; Neueder, R.; Kunz, W. *Langmuir* **2003**, *19*, 8226.
(7) Gradzielski, M. *Curr. Opin. Colloid Interface Sci.* **2004**, *9*, 256.
(8) Bresme, F.; Faraudo, J. *Langmuir* **2004**, *20*, 5127.
(9) Sammalkorpi, M.; Karttunen, M.; Haataja, M. *J. Chem. Phys. B* **2007**, *111*, 11722.
(10) Shi, W.-X.; Guo, H.-X. *J. Chem. Phys. B* **2010**, *114*, 6365.
(11) Jusufi, A.; Hynninen, A.-P.; Haataja, M.; Panagiotopoulos, A. Z. *J. Chem. Phys. B* **2009**, *113*, 6314.
(12) Sammalkorpi, M.; Karttunen, M.; Haataja, M. *J. Chem. Phys. B* **2009**, *113*, 5863.
(13) Israelachvili, J. N. *Intermolecular and Surface Forces*, 2nd ed.; Academic Press: New York, 1991.
(14) Sadus, R. J. *Mol. Simul.* **2006**, *32*, 185.
(15) Binder, K. *Phys. Rev. A* **1982**, *25*, 1699.
(16) Mecke, M.; Winkelmann, J.; Fischer, J. *J. Chem. Phys.* **1997**, *107*, 9264.
(17) Errington, J. R.; Kofke, D. A. *J. Chem. Phys.* **2007**, *127*, 174709.
(18) Biscay, F.; Ghoufi, A.; Goujon, F.; Lachet, V.; Malfreyt, P. *J. Chem. Phys. B* **2008**, *112*, 13885.
(19) Kirkwood, J. G.; Buff, F. P. *J. Chem. Phys.* **1949**, *17*, 338.
(20) Ismail, A. E.; Tsige, M.; In, P. J. V.; Grest, G. S. *Mol. Phys.* **2007**, *105*, 3155.
(21) Feng, C.; Paul, E. S. *J. Chem. Phys.* **2007**, *126*, 221101.
(22) Dominguez, H.; Berkowitz, M. L. *J. Chem. Phys. B* **2000**, *104*, 5302.
(23) Jang, S. S.; Lin, S. T.; Maiti, P. K.; Blanco, M.; Goddard, W. A.; Shuler, P.; Tang, Y. *J. Phys. Chem. B* **2004**, *108*, 12130.
(24) Jang, S. S.; Goddard, W. A. *J. Chem. Phys. B* **2006**, *110*, 7992.
(25) Lamoureux, G.; Roux, B. *J. Chem. Phys. B* **2006**, *110*, 3308.
(26) Bucher, D.; Kuyucak, S. *J. Chem. Phys. B* **2008**, *112*, 10786.
(27) Krekeler, C.; Hess, B.; Site, L. D. *J. Chem. Phys.* **2006**, *125*, 054305.
(28) Schweighofer, K. J.; Essmann, U.; Berkowitz, M. *J. Chem. Phys. B* **1997**, *101*, 3793.
(29) Dominguez, H. *J. Colloid Interface Sci.* **2004**, *274*, 665.
(30) Dominguez, H.; Rivera, M. *Langmuir* **2005**, *21*, 7257.
(31) Bresme, F.; Faraudo, J. *Mol. Simul.* **2006**, *32*, 1103.
(32) Dominguez, H. *J. Chem. Phys. B* **2006**, *110*, 13151.
(33) Dominguez, H. *J. Phys. Chem. B* **2007**, *111*, 4054.
(34) Hantal, G.; Partay, L. B.; Varga, I.; Jedlovszky, P.; Gilanyi, T. *J. Chem. Phys. B* **2007**, *111*, 1769.
(35) Stephenson, B. C.; Beers, K. J.; Blankschtein, D. *J. Chem. Phys. B* **2007**, *111*, 1063.
(36) Stephenson, B. C.; Stafford, K. A.; Beers, K. J.; Blankschtein, D. *J. Phys. Chem. B* **2008**, *112*, 1641.
(37) Tummala, N. R.; Striolo, A. *J. Phys. Chem. B* **2008**, *112*, 1987.
(38) Yang, W. H.; Wu, R. L.; Kong, B.; Zhang, X. F.; Yang, X. Z. *J. Phys. Chem. B* **2009**, *113*, 8332.
(39) Patra, M.; Karttunen, M. *J. Comput. Chem.* **2004**, *25*, 678.
(40) Fennell, C. J.; Bizjak, A.; Vlachy, V.; Dill, K. A. *J. Chem. Phys. B* **2009**, *113*, 6782.
(41) Hess, B.; Holm, C.; Vegt, N. v. d. *J. Chem. Phys.* **2006**, *124*, 164509.
(42) Auffinger, P.; Cheatham, T. E.; Vaiana, A. C. *J. Chem. Theory. Comput.* **2007**, *3*, 1851.
(43) Martin, M. G.; Siepmann, J. I. *J. Phys. Chem. B* **1998**, *102*, 2569.
(44) Berendsen, H. J. C.; Grigera, J. R.; Straatsma, T. P. *J. Chem. Phys.* **1987**, *91*, 6269.
(45) Joung, I. S.; Cheatham, T. E. *J. Chem. Phys. B* **2008**, *112*, 9020.
(46) Cornell, W. D.; Cieplak, P.; Bayly, C. I.; Gould, I. R.; Merz, K. M.; Ferguson, D. M.; Spellmeyer, D. C.; Fox, T.; Caldwell, J. W.; Kollman, P. A. *J. Am. Chem. Soc.* **1995**, *117*, 5179.
(47) Tolman, R. C. *J. Chem. Phys.* **1948**, *16*, 758.
(48) Martínez, L.; Andrade, R.; Birgin, E. G.; Martínez, J. M. *J. Comput. Chem.* **2009**, *30*, 2157.
(49) Kirkwood, J. G.; Buff, F. P. *J. Chem. Phys.* **1951**, *19*, 774.

(50) Weerasinghe, S.; Smith, P. E. *J. Chem. Phys.* **2003**, *119*, 11342.
(51) Gampe, T.; Libuś, Z. *J. Solution Chem.* **1999**, *28*, 837.
(52) Spoel, D. V. D.; Lindahl, E.; Hess, B.; Groenhof, G.; Mark, A. E.; Berendsen, H. J. C. *J. Comput. Chem.* **2005**, *26*, 1701.
(53) Berendsen, H. J. C.; Postma, J. P. M.; Gunsteren, W. F. v.; DiNola, A.; Haak, J. R. *J. Chem. Phys.* **1984**, *81*, 3684.
(54) Tom, D.; Darrin, Y.; Lee, P. *J. Chem. Phys.* **1993**, *98*, 10089.
(55) Orea, P.; López-Lemus, J.; Alejandre, J. *J. Chem. Phys.* **2005**, *123*, 114702.
(56) Gonzalez-Melchor, M.; Orea, P.; Lopez-Lemus, J.; Bresme, F.; Alejandre, J. *J. Chem. Phys.* **2005**, *122*, 094503.
(57) Trokhymchuk, A.; Alejandre, J. *J. Chem. Phys.* **1999**, *111*, 8510.
(58) López-lemus, J.; Alejandre, J. *Mol. Phys.* **2002**, *100*, 2983.
(59) Goujon, F.; Malfreyt, P.; Boutin, A.; Fuchs, A. H. *J. Chem. Phys.* **2002**, *116*, 8106.
(60) Grosfils, P.; Lutsko, J. F. *J. Chem. Phys.* **2009**, *130*, 054703.
(61) Goujon, F.; Malfreyt, P.; Simon, J.-M.; Boutin, A.; Rousseau, B.; Fuchs, A. H. *J. Chem. Phys.* **2004**, *121*, 12559.
(62) Ibergay, C.; Ghoufi, A.; Goujon, F.; Ungerer, P.; Boutin, A.; Rousseau, B.; Malfreyt, P. *Phys. Rev. E* **2007**, *75*, 051602.
(63) Biscay, F.; Ghoufi, A.; Goujon, F.; Lachet, V.; Malfreyt, P. *J. Chem. Phys.* **2009**, *130*, 184710.
(64) Shen, V. K.; Mountain, R. D.; Errington, J. R. *J. Chem. Phys. B* **2007**, *111*, 6198.
(65) Biscay, F.; Ghoufi, A.; Lachet, V.; Malfreyt, P. *J. Chem. Phys.* **2009**, *131*, 124707.
(66) Fennell, C. J.; Bizjak, A.; Vlachy, V.; Dill, K. A.; Sarupria, S.; Rajamani, S.; Garde, S. *J. Chem. Phys. B* **2009**, *113*, 14837.
(67) Kalcher, I.; Dzubiella, J. *J. Chem. Phys.* **2009**, *130*, 134507.
(68) Poghosyan, A. H.; Yeghiazaryan, G. A.; Gharabekyan, H. H.; Koetz, J.; Shahinyan, A. A. *Mol. Simul.* **2007**, *33*, 1155.
(69) Egberts, E.; Berendsen, H. J. C. *J. Chem. Phys.* **1988**, *89*, 3718.
(70) Hore, D. K.; Beaman, D. K.; Richmond, G. L. *J. Am. Chem. Soc.* **2005**, *127*, 9356.
(71) Zhao, T.; Xu, G.; Yuan, S.; Chen, Y.; Yan, H. *J. Chem. Phys. B* **2010**, *114*, 5025.
(72) Howes, A. J.; Radke, C. J. *Langmuir* **2007**, *23*, 1835.

JP107002X